CRB-Based Design of Linear Antenna Arrays for Near-Field Source Localization

Houcem Gazzah and Jean Pierre Delmas, *Senior Member, IEEE*

***Abstract*—This paper is devoted to the Cramer Rao bound (CRB) on the angle and range of a narrow-band near-field source localized by means of an arbitrary linear array using the exact expression of the time delay parameter. First, we prove that the conditional and unconditional CRBs are proportional for an arbitrary parametrization of the steering vector (that may include, but is not limited to, the source DOA, range or polarization). Then, a Taylor expansion of the CRB is conducted to obtain accurate nonmatrix closed-form expressions of the CRB on angle and range. In contrast to the existing expressions, our expressions are simple, interpretable and more general because the sensors are only constrained to be placed along some axis. Our analysis leads to the characterization and design of a class of *centro-symmetric* linear arrays with improved near-field angle and range estimation capabilities.**

***Index Terms*—Cramer Rao bounds, linear antenna arrays, direction-of-arrival and range estimation, near-field source localization.**

I. Introduction

UNIFORM LINEAR ARRAYS (ULA) are the most commonly used type of linear antenna arrays because they are ambiguity-free and allow for fast estimation algorithms, when we look for the direction of arrival (DOA) of far-field sources. However, when the source is located in the antenna near-field, a change of the signal model occurs as a new parameter is to be taken into consideration: the source-to-antenna distance. Fast algorithms are no longer applicable, and, more seriously, the new (range) parameter affects DOA estimation accuracy, and, for some applications, is itself a parameter of interest that needs to be estimated. In this context, we prove that the ULA configuration is not the best one anymore. Alternative (other than uniform) ways of placing the sensors are shown to improve range estimation accuracy.

To motivate our design, we adopt as a performance measure the algorithm-independent CRB which constitutes the minimum achievable variance on the estimated source parameters, here DOA and range of the near-field source. Despite the huge literature about DOA estimation [1], research has been mostly dedicated to far-field sources. In fact, when the source is in the array far-field, the (planar) waveform reaches two sensors with a time difference that is proportional to the spacing between the two sensors. Hence, it is possible to obtain simple and interpretable nonmatrix expressions for the CRB (see, e.g., [2]). In contrast, when the source is in the antenna near-field, the time delay expression is more intricate and only approximate nonmatrix expressions of this CRB have been obtained. Based on an approximate propagation model, early near-field CRBs expressions have been obtained using second-order Taylor expansion of the time delay parameter [3], [4]. Only lately has the exact time delay formula been used [5], but only to calculate the near-field CRB of the ULA.

We start by underlying a fact about the so-called conditional and unconditional CRBs. Often, they have been considered as independent (e.g., recent papers [6] and [5] conclude by "extension of this work for stochastic sources is under consideration"). In this paper, we show that they are, actually, proportional, an issue previously overlooked. Then, we develop accurate nonmatrix expressions of the CRB on both DOA and range, using linear arrays of arbitrarily spaced sensors. They are more general than those of [5] because we do not assume uniform linear arrays (neither punctured nor sparse) where intersensor spacings[1] are multiples of a fixed minimum distance [9]. They are also more compact than those from [4], [5], and [10] if applied to the special case of ULA, and so thanks to a different coordinate system that implies a different definition of DOA and range.

The obtained CRB expressions allow for a rich interpretation of the array estimation capabilities when the source is in the antenna near-field. For instance, they highlight the interest of a class of *centro-symmetric* linear arrays made of pairs of sensors symmetrically located along the two sides of the linear antenna array. Attractive features of such centro-symmetric linear arrays include lower DOA and range CRBs and faster convergence to the lower far-field DOA CRB. Also, we show that within centro-symmetric linear arrays, ULA is not the best choice. Centro-symmetric linear arrays are designed that achieve identical DOA CRB as the ULA but significantly lower range CRB (by as much as 50%). For instance, a geometric parameter is identified that controls the near-field estimation performance of the centro-symmetric linear array.

The paper is organized as follows. Section II formulates the problem and specifies the data model. Section III is dedicated to new expressions of the CRB. First, assuming an arbitrary parametrization of the steering vector, we prove that the conditional and unconditional CRBs are proportional. Then, we focus on DOA and range estimation of near-field sources. Using

Manuscript received September 08, 2013; revised December 22, 2013; accepted December 30, 2013. Date of publication January 09, 2014; date of current version April 03, 2014.

H. Gazzah is with the Department of Electrical and Computer Engineering, University of Sharjah, Sharjah 27272, UAE (e-mail: hgazzah@sharjah.ac.ae).

J. P. Delmas is with the Department CITI, Telecom SudParis, Evry 91011, France (e-mail: jean-pierre.delmas@it-sudparis.eu).

Digital Object Identifier 10.1109/TAP.2014.2298882

[1]Constraints on the array positions, often adopted to limit array ambiguities [7], may, at the same time, affect estimation performance [8].

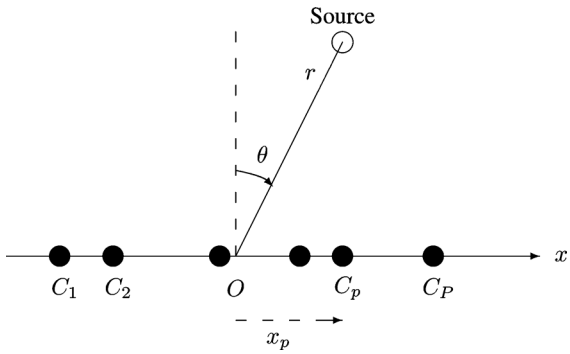

Fig. 1. Source in the near-field of the arbitrary linear array.

Taylor expansion, new expressions of the CRB are derived, and numerically validated. The important class of centro-symmetric arrays is studied in details in Section IV where better-than-ULA arrays are obtained. The paper is concluded in Section V.

II. Data Model

As depicted in Fig. 1, we consider a linear antenna array made of P sensors $C_1, \ldots, C_P$. They are located along a straight line at coordinates $x_1, \ldots, x_P$, respectively. Without loss of generality, we assume the array centroid to be at the origin O of this axis. Opportunistically, this choice allows for more compact expressions of the CRB, compared to [4], [5]. A narrow-band signal $s(t)$, with wavelength λ, is emitted towards the antenna array by a source S located at a range r from the origin O and forming an angle θ with the axis orthogonal to the array. The snapshot collected by sensor p at time index t is

$$y_p(t) = g_p \exp(i\tau_p) s(t) + n_p(t),$$

where $s(t)$ and $n_p(t)$ represent, respectively, the source signal collected at the origin and the ambient additive noise collected by sensor p. Amplitude g_p may depend on both r and θ, while phase τ_p, defined as $\tau_p = 2\pi(SO - SC_p)/\lambda$, can be rewritten as

$$\tau_p = 2\pi \frac{r}{\lambda}(1 - \sqrt{\beta_p})$$

with $\beta_p \overset{\text{def}}{=} 1 - 2(x_p)/(r)\sin(\theta) + (x_p^2)/(r^2)$. Based on N snapshots $\{y_p(t)\}_{p=1,\ldots,P;t=t_1,\ldots,t_N}$, estimates of both the range r and the DOA θ are obtained by means of a variety of algorithms, among which a few are capable of achieving the stochastic CRB [11].

Estimation accuracy is evaluated in terms of the CRB, under the usual statistical assumptions about $n_p(t)$ and $s(t)$: 1) $n_p(t)$ and $s(t)$ are independent; 2) $\{n_p(t)\}_{p=1,\ldots,P;t=t_1,\ldots,t_N}$ are independent, zero-mean, circular and Gaussian distributed with variance σ_n^2; and 3) $\{s(t)\}_{t=t_1,\ldots,t_N}$ are assumed to be either deterministic unknown parameters (the so-called conditional or deterministic model), or independent zero-mean circular Gaussian distributed with variance σ_s^2 (the so-called unconditional or stochastic model).

III. Expressions of the CRB

A. A General Result About the CRB

We prove that the stochastic and deterministic CRBs are equal, up to a multiplicative constant, in the specific case of a single source.

To introduce the two types of CRBs, we consider a more general signal model with an arbitrary number K of sources (with $K < p$) and an arbitrary parametrization $\boldsymbol{\alpha} = [\alpha_1, \ldots, \alpha_L]^T$ of the steering vectors $\mathbf{a}_k(\boldsymbol{\alpha})$ related to array geometry or polarization, defined by

$$[\mathbf{a}_k(\boldsymbol{\alpha})]_{p=1\ldots P} = g_{p,k} e^{i\tau_{p,k}}$$

where $g_{p,k}$ and $\tau_{p,k}$ denote the gain and the phase of the p-th sensor associated with the k-th source, w.r.t. the origin O. $g_{p,k}$ includes in particular possible power profiles and/or directional gains.

General compact expressions of the CRB, concentrated on the parameters of the K steering vectors alone, have been derived for these two models of sources (see e.g., [12]) for one parameter per source. The expression of the stochastic CRB has been extended for several parameters per source in ([13], Appendix D), and following the proof given in [12], the expression of the deterministic CRB can be also extended to several parameters per source. These expressions are given respectively by

$$\mathrm{CRB}_{\mathrm{sto}}(\boldsymbol{\alpha}) = \frac{\sigma_n^2}{2N}\left[\mathrm{Re}\left(\mathbf{H} \odot \left(\left(\mathbf{R}_s \mathbf{A}^H \mathbf{R}_y^{-1} \mathbf{A} \mathbf{R}_s\right)^T \otimes \mathbf{1}_L\right)\right)\right]^{-1} \quad (1)$$

$$\mathrm{CRB}_{\mathrm{det}}(\boldsymbol{\alpha}) = \frac{\sigma_n^2}{2N}\left[\mathrm{Re}\left(\mathbf{H} \odot \left(\mathbf{R}_s^T \otimes \mathbf{1}_L\right)\right)\right]^{-1}. \quad (2)$$

There, $\mathbf{R}_y \overset{\text{def}}{=} \mathrm{E}[\mathbf{y}(t)\mathbf{y}^H(t)]$ with $\mathbf{y}(t) \overset{\text{def}}{=} [y_1(t), \ldots, y_P(t)]^T$ and $\mathbf{A} \overset{\text{def}}{=} [\mathbf{a}_1, ..., \mathbf{a}_P]$. With $\mathbf{s}(t) \overset{\text{def}}{=} [s_1(t), \ldots, s_K(t)]^T$, we define $\mathbf{R}_s$ as $\mathrm{E}[\mathbf{s}(t)\mathbf{s}^H(t)]$ in (1) and as $(1/N)\sum_{n=1}^N \mathbf{s}(t_n)\mathbf{s}^H(t_n)$ in (2). Also, $\mathbf{H} \overset{\text{def}}{=} \mathbf{D}^H[\mathbf{I} - \mathbf{A}(\mathbf{A}^H\mathbf{A})^{-1}\mathbf{A}^H]\mathbf{D}$ and $\mathbf{D} \overset{\text{def}}{=} [d\mathbf{a}_1/d\boldsymbol{\alpha}_1, \ldots, d\mathbf{a}_K/d\boldsymbol{\alpha}_K]$. Symbols $\otimes$, $\odot$ and $\mathbf{1}_L$ represent the Kronecker product, the Hadamard product and the $L \times L$ matrix of 1 s, respectively.

Specialized to a single source for which $\mathbf{R}_y = \sigma_s^2 \mathbf{a}(\boldsymbol{\alpha})\mathbf{a}^H(\boldsymbol{\alpha}) + \sigma_n^2 \mathbf{I}$ where $\sigma_s^2 \overset{\text{def}}{=} (1/N)\sum_{n=1}^N |s(t_n)^2|$ for the deterministic model of the source, it is straightforward to see that

$$\begin{aligned}\mathrm{CRB}_{\mathrm{sto}}(\boldsymbol{\alpha}) &= \left(1 + \frac{\sigma_n^2}{\|\mathbf{a}(\boldsymbol{\alpha})\|^2 \sigma_s^2}\right)\mathrm{CRB}_{\mathrm{det}}(\boldsymbol{\alpha}) \quad (3)\\ &= [\mathbf{F}(\boldsymbol{\alpha})]^{-1}\end{aligned}$$

where

$$\begin{aligned}\mathbf{F}(\boldsymbol{\alpha}) = c_\sigma(\boldsymbol{\alpha})[&\|\mathbf{a}(\boldsymbol{\alpha})\|^2 \mathbf{D}^H(\boldsymbol{\alpha})\mathbf{D}(\boldsymbol{\alpha})\\ &- \mathbf{D}^H(\boldsymbol{\alpha})\mathbf{a}(\boldsymbol{\alpha})\mathbf{a}^H(\boldsymbol{\alpha})\mathbf{D}(\boldsymbol{\alpha})] \quad (4)\end{aligned}$$

with $\mathbf{D}(\boldsymbol{\alpha}) \overset{\text{def}}{=} [\partial\mathbf{a}(\boldsymbol{\alpha})/\partial\alpha_1, \ldots, \partial\mathbf{a}(\boldsymbol{\alpha})/\partial\alpha_L]$ and where $c_\sigma(\boldsymbol{\alpha}) \overset{\text{def}}{=} 2N\sigma_s^4/[\sigma_n^2(\sigma_n^2 + \|\mathbf{a}(\boldsymbol{\alpha})\|^2\sigma_s^2)]$ is independent from the source and sensors positions for constant modulus steering vectors, only.

Thanks to (3), we will only consider the stochastic source model for which the elements of matrix $\mathbf{F}$ in (4) are proved to be equal to

$$\frac{\mathbf{F}_{ij}}{c_\sigma(\boldsymbol{\alpha})} = \left(\sum_{p=1}^{P} g_p^2\right)\left(\sum_{p=1}^{P} g'_{p,i}g'_{p,j} + \tau'_{p,i}\tau'_{p,j}g_p^2\right) - \left(\sum_{p=1}^{P} g'_{p,i}g_p\right)\left(\sum_{p=1}^{P} g'_{p,j}g_p\right) - \left(\sum_{p=1}^{P} \tau'_{p,i}g_p^2\right)\left(\sum_{p=1}^{P} \tau'_{p,j}g_p^2\right)$$

where $g'_{p,i}$ and $\tau'_{p,i}$ are derivatives of g_p and τ_p w.r.t. α_i, respectively.

Should the gain g_p be the same for all sensors, denoted then as $g_p = g(\boldsymbol{\alpha})$, the general expression above can be greatly simplified. After some algebraic manipulations, the following can be proved:

$$\frac{\mathbf{F}_{ij}}{c'_\sigma(\boldsymbol{\alpha})} = P\sum_{p=1}^{P} \tau'_{p,i}\tau'_{p,j} - \left(\sum_{p=1}^{P} \tau'_{p,i}\right)\left(\sum_{p=1}^{P} \tau'_{p,j}\right) \quad (5)$$

where now $c'_\sigma(\boldsymbol{\alpha}) \stackrel{\text{def}}{=} 2N\sigma_s^4 g^4(\boldsymbol{\alpha})/[\sigma_n^2(\sigma_n^2 + Pg^2(\boldsymbol{\alpha})\sigma_s^2)]$. In this case, the CRB, denoted as $\mathrm{CRB}^{\mathrm{DIR}}(\boldsymbol{\alpha})$, is related to the CRB associated with an array of isotropic sensors (for which $g_p = 1$). In fact, if the latter is denoted as $\mathrm{CRB}^{\mathrm{ISO}}(\boldsymbol{\alpha})$, then we can prove the following

$$\mathrm{CRB}^{\mathrm{DIR}}(\boldsymbol{\alpha}) = \frac{1}{g^4(\boldsymbol{\alpha})}\frac{1 + Pg^2(\boldsymbol{\alpha})\frac{\sigma_s^2}{\sigma_n^2}}{1 + P\frac{\sigma_s^2}{\sigma_n^2}}\mathrm{CRB}^{\mathrm{ISO}}(\boldsymbol{\alpha}). \quad (6)$$

Apart from these two quite related cases, it is not trivial to study antenna arrays made of nonisotropic differently-oriented sensors. This is especially relevant for the near-field region because different sensors shouldn't experience the same gain as a result of them seeing the source from different angles and being located at different distances from the source.

B. Taylor Expansion of the Near-Field $\mathbf{F}$ Matrix

In the addressed problem, $\alpha_1 = \theta$ and $\alpha_2 = r$. As often assumed in the CRB literature, we consider a unitary modulus gain[2]. Hence, (5) holds and $c'_\sigma(\boldsymbol{\alpha})$, simplified to $c_\sigma = 2N\sigma_s^4/[\sigma_n^2(\sigma_n^2 + P\sigma_s^2)]$, is independent from the source and sensors positions. The following Taylor expansion of matrix $\mathbf{F}$ in (5) is proved in Appendix A:

$$\frac{2c}{r\cos^3(\theta)}\mathbf{F}_{12} = P\frac{S_3}{r^3} + \sin(\theta)\frac{3PS_4 - S_2^2}{r^4} + o(\epsilon^4) \quad (7)$$

[2]This condition, stronger than $\|\mathbf{a}(\boldsymbol{\alpha})\|^2 = P$, corresponds to omnidirectional sensors.

$$\frac{c}{r^2\cos^2(\theta)}\mathbf{F}_{11} = P\frac{S_2}{r^2} + 2P\sin(\theta)\frac{S_3}{r^3} + \frac{S_4P[4\sin^2(\theta) - 1] - S_2^2\sin^2(\theta)}{r^4} + o(\epsilon^4), \quad (8)$$

while F_{22} is shown in (9) at the bottom of this page. There $\epsilon \stackrel{\text{def}}{=} \max_p |x_p|/r$, $\lim_{\epsilon\to 0} o(\epsilon)/\epsilon = 0$, $c \stackrel{\text{def}}{=} \lambda^2/(4\pi^2 c_\sigma)$ and $S_k \stackrel{\text{def}}{=} \sum_{p=1}^{P} x_p^k$ are array geometry dependent constants, with, in particular, $S_1 = 0$.

C. Taylor Expansion of the Near-Field CRB

From the expression (7) of matrix $\mathbf{F}$, we see that the most significant term is equal to zero if and only if $S_3 = 0$. This can be interpreted as a necessary (and, in practice, sufficient) condition on the array geometry to ensure a decoupling between the DOA and range estimates to the second-order in ϵ. This special, yet important case, will be studied in details in Section IV. For the moment, we give results about the general case of antenna arrays for which S_3 is not necessarily zero.

Starting from matrix $\mathbf{F}$ as it appears in (7)–(9), and following steps summarized in Appendix B, the next expressions of the CRB on the DOA and range are obtained:

$$\mathrm{CRB}(\theta) = \frac{c}{P}\frac{1}{S_2 - \frac{PS_3^2}{PS_4 - S_2^2}}\frac{1 + \gamma_1\frac{\sin(\theta)}{r}}{\cos^2(\theta)} + o(\epsilon), \quad (10)$$

$$\frac{\mathrm{CRB}(r)}{r^4} = \frac{4c}{PS_4 - S_2^2 - P\frac{S_3^2}{S_2}}\frac{1 + \gamma_2\frac{\sin(\theta)}{r}}{\cos^4(\theta)} + o(\epsilon) \quad (11)$$

where $\gamma_1 \stackrel{\text{def}}{=} 4PS_3(S_2S_3^2 - S_2^2S_4 + PS_4^2 - PS_3S_5)/[(PS_4 - S_2^2)(PS_2S_4 - S_3^2 - PS_3^2)]$ and $\gamma_2 \stackrel{\text{def}}{=} 2(3PS_2S_3S_4 + S_2^2S_3 - PS_3^3 - 2PS_2^2S_5)/[S_2(PS_2S_4 - S_3^2 - PS_3^2)]$. Both depend on S_2, S_3, S_4 and S_5, but not on S_6, contrarily to CRBs obtained in the next section.

D. The Case of Centro-Symmetric Arrays

Note that if $S_3 = 0$ (resp., if $S_3 = S_5 = 0$), the expression (10) [resp., (11)] is still valid. However, the term in $1/r$ in (10) of $\mathrm{CRB}(\theta)$ [resp., in (11) of $\mathrm{CRB}(r)$] vanishes. This scenario is far from being marginal, as it notably includes the ULA. Specific results are developed to cover such arrays. We will discuss, in particular, the so-called *centro-symmetric* arrays, ones for which if a sensor is placed at some position x_p, then another one is placed at coordinate $-x_p$.

Under the condition $S_3 = 0$ (resp., $S_3 = S_5 = 0$), γ_1 (resp. γ_2) disappears from (10) [resp., from (11)] and so disappears r. The Taylor expansion has to be pushed one step further to unveil

$$\frac{c}{\cos^4(\theta)}\mathbf{F}_{22} = \frac{1}{4}\frac{PS_4 - S_2^2}{r^4} + \frac{PS_5 - S_2S_3}{r^5}\sin(\theta) + \frac{PS_6\left[23\sin^2(\theta) - 3\right] - 3S_2S_4\left[5\sin^2(\theta) - 1\right] - 8S_3^2\sin^2(\theta)}{8r^6} + o(\epsilon^6), \quad (9)$$

its dependence on ϵ, i.e., on range r. In fact, enforcing $S_3 = 0$ in (7)–(9) leads to

$$\frac{2c}{r\cos^3(\theta)}\mathbf{F}_{12} = \sin(\theta)\frac{3PS_4 - S_2^2}{r^4} + o(\epsilon^4) \quad (12)$$

$$\frac{c}{r^2\cos^2(\theta)}\mathbf{F}_{11} = P\frac{S_2}{r^2} + \frac{S_4P\left[4\sin^2(\theta) - 1\right] - S_2^2\sin^2(\theta)}{r^4} + o(\epsilon^4), \quad (13)$$

while F_{22} is shown in (14) at the bottom of this page. The above matrix is inverted while, this time, keeping track of terms in ϵ^2 (more details in Appendix C). At the end, we prove that, for antenna arrays with $S_3 = 0$, we have

$$\mathrm{CRB}(\theta) = c\frac{1 + \left[1 + \left(1 + \frac{4PS_4}{PS_4 - S_2^2}\right)\sin^2(\theta)\right]\frac{S_4}{S_2}\frac{1}{r^2}}{\cos^2(\theta)PS_2} + o(\epsilon^2). \quad (15)$$

While, for antenna arrays that satisfy both $S_3 = 0$ and $S_5 = 0$, we have

$$\frac{\mathrm{CRB}(r)}{r^4} = c\frac{1}{\cos^4(\theta)}\frac{4}{PS_4 - S_2^2} \times \left[1 + \frac{\gamma_3(\theta)}{2\left(PS_4 - S_2^2\right)r^2}\right] + o(\epsilon^2) \quad (16)$$

where $\gamma_3(\theta) \stackrel{\mathrm{def}}{=} [(18P^2S_4^2 + 2S_2^4 + 3PS_2^2S_4 - 23P^2S_2S_6)/(PS_2)] \times \sin^2(\theta) + 3PS_6 - 3S_2S_4$.

E. Numerical Validation

Let us, first, highlight similarities between the obtained CRBs (10), (11), (15) and (16). For this purpose we define $C_1 \stackrel{\mathrm{def}}{=} (1/c)\mathrm{CRB}(\theta)$ and $C_2 \stackrel{\mathrm{def}}{=} [1/(cr^4)]\mathrm{CRB}(r)$, which also have the advantage of not depending on the noise and signal power, nor on the signal wavelength. They are purely geometrical functions of the only sensors and source positions.

For arbitrary linear arrays, (10) and (11) can be rewritten using the unique expression

$$C_i = \frac{T_i^{(1)}}{\cos^{2i}(\theta)}\left[1 + T_i^{(2)}\frac{\sin(\theta)}{r}\right] + o(\epsilon)$$

Expressions of constants $T_i^{(1)}$ and $T_i^{(2)}$ can be easily found and depend only on the array sensor positions. For centro-symmetric arrays (more explicitly, for arrays satisfying $S_3 = 0$ for C_1 and $S_3 = S_5 = 0$ for C_2), unified expressions can be found as well. Indeed, (15) and (16) are rewritten as a unique expression

$$C_i = \frac{T_i^{(3)}}{\cos^{2i}(\theta)}\left[1 + \left(T_i^{(4)}\sin^2(\theta) + T_i^{(5)}\right)\frac{T_i^{(6)}}{r^2}\right] + o(\epsilon^2)$$

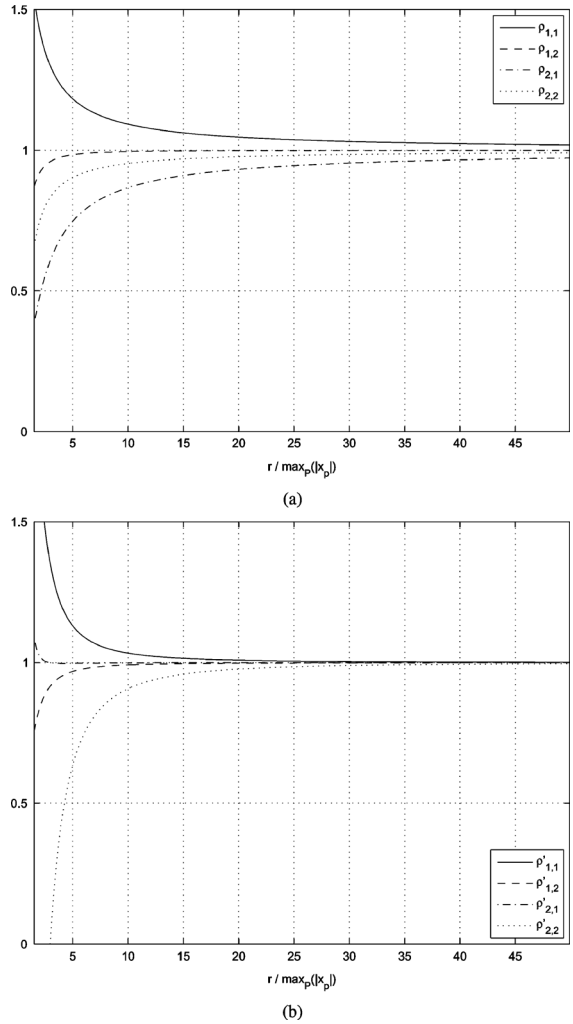

Fig. 2. Validation of the DOA and range CRBs for an increasing source-to-array distance. The array is made of 6 sensors. In (a), they are placed at $-0.1672, -0.0737, 0.0960, -0.1444, 0.4694$ and -0.1801, forming a noncentro-symmetric array. In (b), they form a ULA. The source is placed, in (a), with $\theta = 47.13°$; and, in (b), with $\theta = 146.64°$.

where constants $T_i^{(3)}, T_i^{(4)}, T_i^{(5)}$ and $T_i^{(6)}$ can be easily verified to depend only on the array sensors positions. We intend to validate every single coefficient in the Taylor expansions in (10), (11), (15), and (16).

First, for arbitrary linear arrays, for $i = 1, 2$, we define $\rho_{1,i} \stackrel{\mathrm{def}}{=} \cos^{2i}(\theta)C_i/T_i^{(1)}$ and $\rho_{2,i} \stackrel{\mathrm{def}}{=} r[\cos^{2i}(\theta)C_i/T_i^{(1)} - 1]/[T_i^{(2)}\sin(\theta)]$. All converge to 1 when $1/\epsilon = r/\max_p|x_p|$ converges to infinity. This is verified in Fig. 2(a) where results are given for a nonuniform linear array. Positions of the sensors have been chosen arbitrarily and happen to verify $S_2 = 0.3162$ and $S_3 = 0.0904$.

$$\frac{c}{\cos^4(\theta)}\mathbf{F}_{22} = \frac{PS_4 - S_2^2}{4r^4} + \frac{PS_5}{r^5}\sin(\theta) + \frac{PS_6\left[23\sin^2(\theta) - 3\right] - 3S_2S_4\left[5\sin^2(\theta) - 1\right]}{8r^6} + o(\epsilon^6). \quad (14)$$

Second, for centro-symmetric arrays, for $i = 1, 2$, we introduce $\rho'_{1,i} \stackrel{\text{def}}{=} \cos^{2i}(\theta) C_i / T_i^{(3)}$ and $\rho'_{2,i} \stackrel{\text{def}}{=} r^2[\cos^{2i}(\theta) C_i / T_i^{(3)} - 1] / [(T_i^{(4)} \sin^2(\theta) + T_i^{(5)}) T_i^{(6)}]$, which, also, converge to 1 when $1/\epsilon = r / \max_p |x_p|$ converges to infinity. This is confirmed by the numerical evaluations for the 6 sensors ULA, reported in Fig. 2(b).

IV. Analysis of Centro-Symmetric Arrays

A. Relations Between Far-Field and Near-Field DOA Performances

CRB expressions (10)–(11) as opposed to CRB expressions (15)–(16) suggest that there are two classes of antenna arrays with different geometrical properties and estimation performance. In particular, we are interested in the so-called centro-symmetric arrays because they have a better far-field estimation performance. To highlight this fact, we connect our near-field DOA CRB (10) and (15) to the stochastic far-field DOA CRB. The latter is given, for arbitrary linear arrays, by [[9], rel. (5)]

$$\mathrm{CRB}_{\mathrm{FF}}(\theta) = \frac{1}{N} \frac{\lambda^2}{8\pi^2 \cos^2(\theta) \frac{S_2}{P} \frac{\sigma_s^2}{\sigma_n^2}} \left(1 + \frac{1}{P \frac{\sigma_s^2}{\sigma_n^2}}\right) = \frac{c}{\cos^2(\theta) P S_2}. \quad (17)$$

Normalized to the above, our near-field DOA CRBs (10) and (15) lead to, respectively

$$\frac{\mathrm{CRB}(\theta)}{\mathrm{CRB}_{\mathrm{FF}}(\theta)} = \frac{1}{1 - \frac{PS_3^2}{PS_2 S_4 - S_2^3}} \left[1 + \frac{\gamma_1 \sin(\theta)}{r} + o(\epsilon)\right], \quad (18)$$

$$\frac{\mathrm{CRB}(\theta)}{\mathrm{CRB}_{\mathrm{FF}}(\theta)} = 1 + \left[\sin^2(\theta)\left(1 + \frac{4PS_4}{PS_4 - S_2^2}\right) + 1\right] \frac{S_4}{S_2} \frac{1}{r^2} + o(\epsilon^2). \quad (19)$$

From (19), we see that arrays for which $S_3 = 0$ (e.g., for centro-symmetric arrays) do achieve $\mathrm{CRB}_{\mathrm{FF}}(\theta)$ when the source-to-array distance tends to infinity. At the same time, estimation of θ and r are decoupled in matrix $\mathbf{F}$ to the second-order in ϵ. In contrast, noncentro-symmetric arrays in (18), for which $S_3 \neq 0$, verify $\lim_{r\to\infty} \mathrm{CRB}(\theta) > \mathrm{CRB}_{\mathrm{FF}}(\theta)$ because $PS_4 - S_2^2 > 0$ (see Section IV-C). This unexpected behavior is explained by the coupling between θ and r in $\mathbf{F}$ to the second-order in ϵ [see (7)]. More precisely, in the former case, the square of $\mathbf{F}_{12}$ tends to zero more rapidly than $\mathbf{F}_{22}$ when r tends to ∞, in contrast to the latter case for which the square of $\mathbf{F}_{12}$ and the term $\mathbf{F}_{22}$ tend to zero with the same speed. Consequently, from a practical point of view, as far as only the DOA parameter is considered, the far-field model of propagation, although approximative, may be preferable to the exact near-field model for noncentro-symmetric arrays with $S_3 \neq 0$.

If we take the range into consideration, the domain of validity of our approximations is larger for centro-symmetric arrays than for arbitrary arrays, as a result of a convergence in $1/r^2$ compared to $1/r$. Furthermore, when comparing (15) and (16) to (10) and (11), we realize that, for centro-symmetric arrays, the CRBs are symmetric w.r.t. positive/negative θ. However, for arbitrary arrays, they are not.

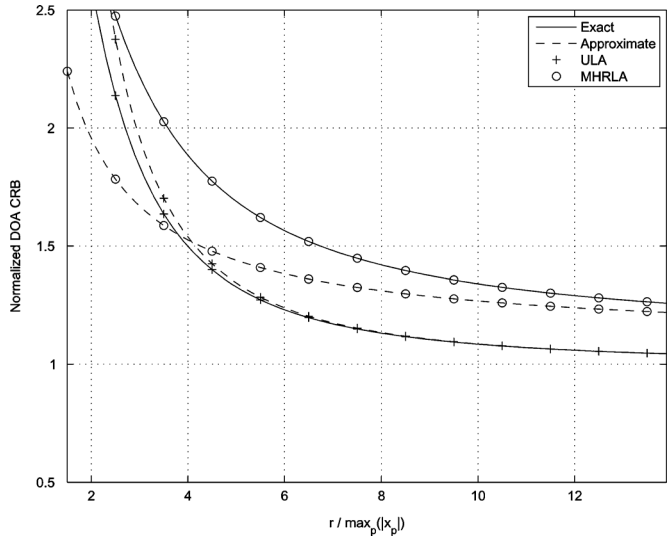

Fig. 3. Approximative and exact ratios $\mathrm{CRB}(\theta)/\mathrm{CRB}_{\mathrm{FF}}(\theta)$ for 4-sensors ULA and MHRLA and a source at $\theta = 60°$. Approximate ratios are calculated using (18) for the (noncentro-symmetric) MHRLA, and (19) for the (centro-symmetric) ULA.

To illustrate the different behavior of centro-symmetric and noncentro-symmetric arrays in the near-field region, we test in Fig. 3 antenna arrays of $P = 4$ sensors forming either: 1) a ULA with a constant intersensors spacing d and for which $S_3 = S_5 = 0$; or 2) a minimum hole and redundancy linear array (MHRLA) with interspacings $d, 3d, 2d$ [14] and for which $S_3 \neq 0$. Thanks to a larger aperture, the MHRLA exhibits a lower far-field CRB, for instance, $\mathrm{CRB}_{\mathrm{FF}}^{\mathrm{MHRLA}}(\theta)/\mathrm{CRB}_{\mathrm{FF}}^{\mathrm{ULA}}(\theta) \approx 0.22$. However, due to the coupling of θ and r in matrix $\mathbf{F}$ of the MHRLA, we have $\lim_{r\to\infty} \mathrm{CRB}(\theta) > \mathrm{CRB}_{\mathrm{FF}}(\theta)$ for this array. Furthermore, this figure confirms that the domain of validity of our approximations is much larger for centro-symmetric arrays than for noncentro-symmetric arrays.

Finally, notice that because we fix the time reference at the centroid of the array (and not at the left-end as in [5]), we obtain simple and much easier to interpret closed-form CRB expressions that contrast with the intricate expressions [see [5], (10)–(11)] that are valid for the only ULA. In particular, we note the monotone behavior of $\mathrm{CRB}(\theta)$ w.r.t. r and the symmetry of $\mathrm{CRB}(\theta)$ and $\mathrm{CRB}(r)$ w.r.t. positive/negative θ with a minimum for $\theta = 0$. Also notice that, due to the change of time reference, our definition of the couple (θ, r) is different from the one in [5] (it is, actually, significantly different if the source is in the very near-field region).

B. Conditions of Centro-Symmetry

By centro-symmetric, we mean that the array is made of pairs of sensors placed at opposite coordinates, i.e., if a sensor is placed at x_p, then another one is placed at $-x_p$. A sensor may be placed at the origin and, then, P is odd. We find that an array is centro-symmetric if

$$S_i = 0 \text{ for all i odd and less or equal to } P.$$

This is proved by induction (see details in Appendix D) thanks to the Newton–Girard formula ([15], pp. 69–74) that allows one to calculate the different S_i in an iterative manner.

C. Key Geometric Parameters for Near-Field Performance

The rewriting of (10)–(16) allows us to point out two geometric parameters that shape the near-field accuracy of antenna arrays. They are the unit-less

$$\kappa \stackrel{\text{def}}{=} \frac{S_2^2}{PS_4} \quad \text{and} \quad \eta \stackrel{\text{def}}{=} \frac{S_2^3}{P^2 S_6}$$

which remain unchanged if either a sensor is added/removed at/from the origin, or, more importantly, if sensor coordinates are scaled by the same constant.[3] Before showing where κ and η appear in the CRB expressions and how they impact them, we highlight some of their intrinsic properties. First, we prove in Appendix E that

$$\eta \leq \kappa \leq 1. \tag{20}$$

Very interesting is the fact that there is (almost) a one-to-one correspondence between κ and η. In fact, we prove in Appendix F that: 1) for $P = 4$ and if $S_1 = S_3 = 0$, we have

$$\eta = \eta_1(\kappa) \stackrel{\text{def}}{=} \frac{1}{\frac{3}{\kappa} - 2} \tag{21}$$

and 2) for $P = 5$ and if $S_1 = S_3 = S_5 = 0$, we have

$$\eta = \eta_2(\kappa) \stackrel{\text{def}}{=} \frac{4}{5\left(\frac{3}{\kappa} - \frac{5}{2}\right)}. \tag{22}$$

For larger P, the two functions [especially $\eta_2(\kappa)$] provide good approximations of the exact η, as validated by Fig. 4.

D. CRB in Terms of κ and η

The two CRBs in (15) and (16) can now be rewritten as follows:

$$\mathrm{CRB}(\theta) = c\frac{\frac{1}{S_2} + \frac{1}{\kappa}\left[\left(1 + \frac{4}{1-\kappa}\right)\sin^2(\theta) + 1\right]\frac{1}{Pr^2}}{\cos^2(\theta)P} + o(\epsilon^2) \tag{23}$$

$$\frac{\mathrm{CRB}(r)}{r^4} = c\frac{1}{\cos^4(\theta)}\frac{4}{S_2^2}\left[\frac{1}{\frac{1}{\kappa} - 1} + \frac{S_2}{2Pr^2} \times \frac{\left(18 + 3\kappa + 2\kappa^2 - \frac{23}{\eta}\right)\sin^2(\theta) + 3\frac{\kappa^2}{\eta} - 3\kappa}{(1-\kappa)^2}\right] + o(\epsilon^2). \tag{24}$$

It becomes clear that while the array far-field (DOA estimation) performance is determined by S_2 only [which concurs with (17)], κ and η play a role in the (DOA and range estimation) near-field performance.

If S_2 is fixed (which has no impact on κ and η), and if we consider the most significant terms[4] of, respectively, (24) and (23), then it becomes clear that the array estimation performance is controlled by κ through, respectively, 1) $1/(1/\kappa - 1)$ (an increasing function of κ); and 2) function $f_\theta(\kappa)$ defined as

$$f_\theta(\kappa) \stackrel{\text{def}}{=} \frac{1}{\kappa}\left[\left(1 + \frac{4}{1-\kappa}\right)\sin^2(\theta) + 1\right] \stackrel{\text{def}}{=} f_1(\kappa)\sin^2(\theta) + f_2(\kappa).$$

The behavior of $f_\theta(\kappa)$, illustrated in Figs. 5 and 6, suggests that, for DOA estimation, an antenna with κ loosely close to $1/2$ ensures limited degradation in all look directions. Values of κ close to, but lower than, $1/2$ are preferred however, because they also lead to better estimation of the range parameter.

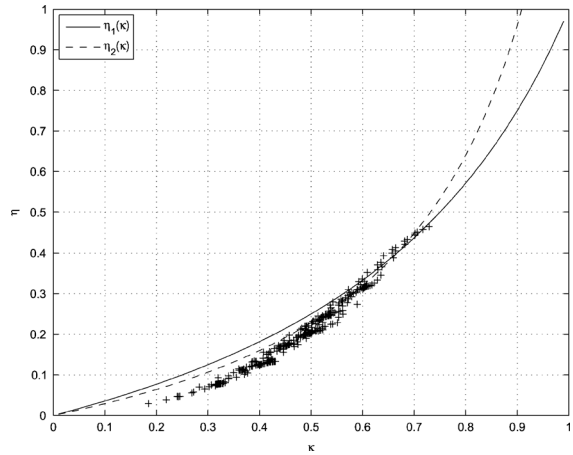

Fig. 4. Systematic search for centro-symmetrical arrays of $P = 15$ sensors verifying $S_2 = 1$. Parameters κ and η are reported as '+' dots, and so in comparison with $\eta_1(\kappa)$ and $\eta_2(\kappa)$.

E. Comparison with ULA

The present analysis shows that, if the source is in the near-field of the linear antenna array, then placing the sensors at a regular spacing will not ensure the best performance. For instance, we prove in Appendix G that, in the case of the ULA, κ tends to $5/9$ (and η converges to $7/27$) if the number of sensors increases to infinity, which, by the way, leads to the following refinements of (23) and (24):

$$\mathrm{CRB}(\theta) \approx \mathrm{CRB}_{\mathrm{FF}}(\theta)\left\{1 + \frac{3P^2d^2}{20r^2}[1 + 10\sin^2(\theta)] + o\left(\frac{P^2d^2}{r^2}\right)\right\},$$

$$\frac{\mathrm{CRB}(r)}{r^4} \approx \frac{720c}{P^6d^4\cos^4(\theta)}\left\{1 + \frac{9P^2d^2}{28r^2}\left[1 - \frac{970}{27}\sin^2(\theta)\right] + o\left(\frac{P^2d^2}{r^2}\right)\right\}$$

where d denotes the spacing between two consecutive sensors.

From the discussion in Section IV-D, a (centro-symmetric) linear antenna with such a value of κ has near-optimum performance for DOA estimation but not for range estimation. To better illustrate the impact of κ on the estimation performance (of both DOA and range), we compare the 6-sensors ULA (with sensors placed at $\pm 0.1195, \pm 0.3586$, and ± 0.5976) against a non-ULA array of 6 sensors located at $\pm 0.0674, \pm 0.2023$ and ± 0.6742. Both arrays exhibit the same $S_2 = 1$ (and, hence,

[3]This property is useful to conduct an affordable systematic search of linear arrays under the nonrestrictive condition $S_2 = 1$.

[4]The first term is the most significant term in (24), for all configurations where $(S_2)/(2Pr^2) < 0.01$, which covers a large domain of practical situations.

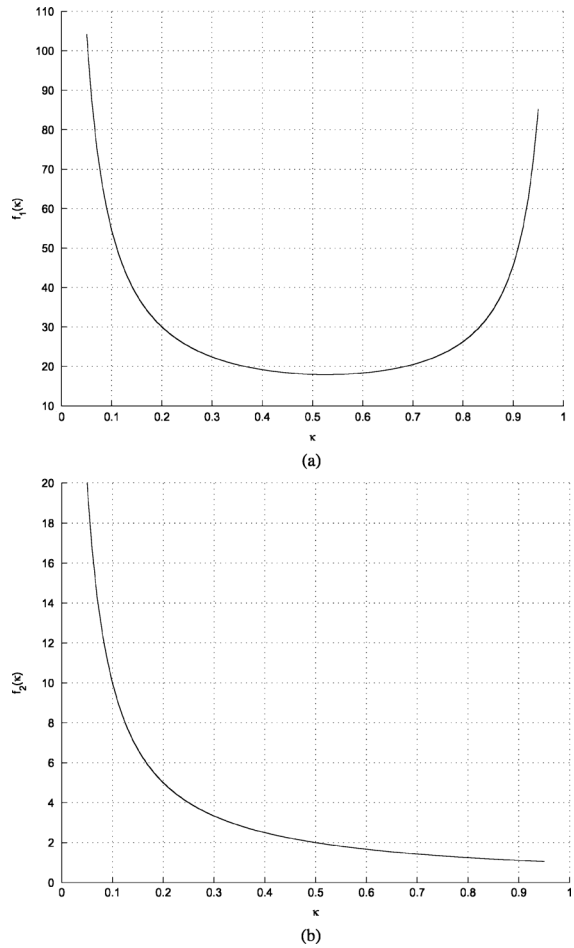

Fig. 5. Near-field DOA estimation performance [expressed by $f_1(\kappa)$ and $f_2(\kappa)$] as function of the geometry of the centro-symmetric array (expressed by parameter κ). (a) $f_1(\kappa)$, (b) $f_2(\kappa)$.

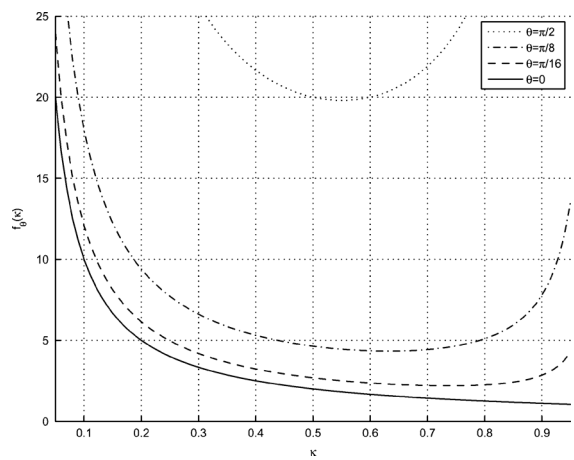

Fig. 6. Near-field DOA estimation performance [expressed by $f_\theta(\kappa)$] as function of the geometry of the centro-symmetric array (expressed by parameter κ), for different look directions.

have identical far-field DOA estimation CRBs). However, κ is equal to 0.5776 for the ULA and to 0.4 for the non-ULA. In Fig. 7, we report the ratios $\mathrm{CRB}(\theta)|_{\mathrm{non-ULA}}/\mathrm{CRB}(\theta)|_{\mathrm{ULA}}$ and $\mathrm{CRB}(r)|_{\mathrm{non-ULA}}/\mathrm{CRB}(r)|_{\mathrm{ULA}}$, calculated using the exact CRB expressions and the approximate CRB expressions in (23) and (24). There, we can see that while we obtain similar DOA performance, the non-ULA array has better range estimation capabilities. Hence, within the family of centro-symmetric linear arrays characterized by a given size P and a given value of S_2, all verify $\lim_{r\to\infty}(\mathrm{CRB}(\theta)|_{\mathrm{non-ULA}}/\mathrm{CRB}(\theta)|_{\mathrm{ULA}}) = 1$, from (23). However, from (24), the κ-dependent function

$$\mathcal{R}_P(\kappa) \stackrel{\mathrm{def}}{=} \lim_{r\to\infty} \frac{\mathrm{CRB}(r)|_{\mathrm{non-ULA}}}{\mathrm{CRB}(r)|_{\mathrm{ULA}}} = \frac{\frac{1}{\kappa_{\mathrm{ULA}}} - 1}{\frac{1}{\kappa} - 1}$$

can be seen as an indicator of improvement (over the ULA) whenever it is lower than one. For instance, if $P \gg 1$

$$\mathcal{R}_P(\kappa) = \frac{4}{5}\frac{1}{\frac{1}{\kappa} - 1}.$$

The above ratio is illustrated in Fig. 8 for the domain[5] [0.3, 0.7] of κ outside which DOA near-field performance degrades severely (as clear from Fig. 6). It can be seen from Fig. 8 that the (far-field) range CRB can be reduced by a much as 50% by antenna arrays with a κ moderately lower than that of the ULA.

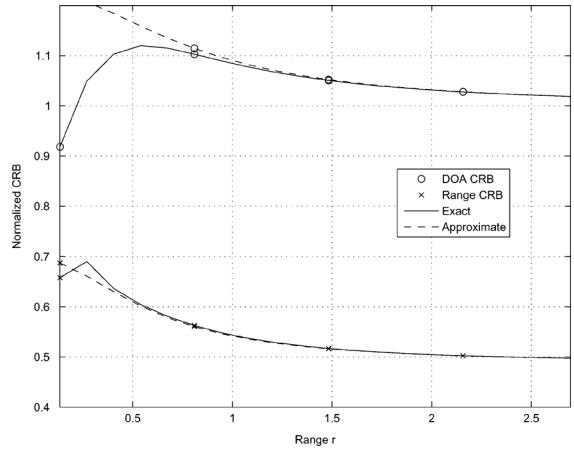

Fig. 7. DOA and range CRBs of the non-ULA ($\kappa = 0.4$) normalized to that of the equivalent ULA ($\kappa = 0.5776$). Both arrays are made of $P = 6$ sensors and are such that $S_2 = 1$.

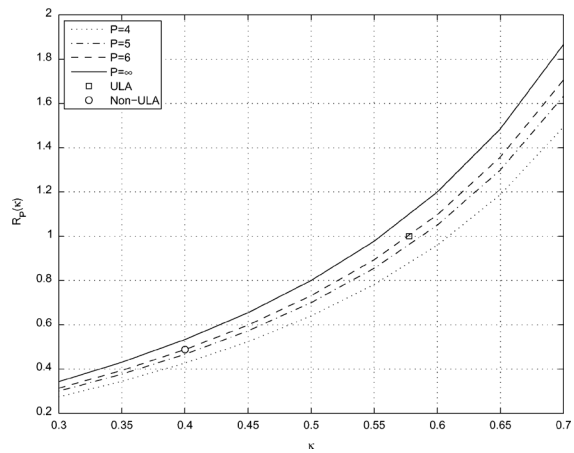

Fig. 8. Centro-symmetric non-ULA versus ULA: Compared range estimation performance of far-field sources.

V. Conclusion

Assuming no constraints other than sensors deployed along a straight line, and using the exact expression of the time delay

[5]In fact, extreme values of κ (i.e., 0 and 1) are achieved by impractically colocalized sensors, either at the origin, or at the same distance (and on both sides) from the origin.

parameter; accurate, simple and interpretable closed-form CRB expressions have been obtained for both angle and range parameters of a near-field narrow-band source.

They show the exact geometric condition for the antenna array to have an attractive behavior in its near-field: better precision and faster convergence to a lower far-field DOA CRB. Such a class of centro-symmetric arrays includes, but is not restricted to, ULAs. Furthermore, it is proved that appropriately designed centro-symmetric non-ULA can largely improve the range estimates without deteriorating the DOA estimates under near-field conditions. Because they potentially have better estimation performance, non-ULAs geometries may be adopted when array ambiguity can be tolerated or counter-measures can be deployed [7]. Hence, our analysis gives a deeper insight into the array near-field performance and shows that more flexibility is available for array design.

APPENDIX

A. Taylor Expansion of $\mathbf{F}$: Proof of (7), (8) and (9)

The main steps of the proof are as follows. First, note that with $\epsilon_p \stackrel{\text{def}}{=} x_p/r$, we have

$$\frac{\lambda}{2\pi}\sum_{p=1}^{P}\tau'_{p,1} = \sum_{p=1}^{P}\cos(\theta) r\frac{\epsilon_p}{\sqrt{\beta_p}},$$

$$\frac{\lambda}{2\pi}\sum_{p=1}^{P}\tau'_{p,2} = P + \sin(\theta)\sum_{p=1}^{P}\frac{\epsilon_p}{\sqrt{\beta_p}} - \sum_{p=1}^{P}\frac{1}{\sqrt{\beta_p}},$$

$$\frac{\lambda^2}{4\pi^2}\sum_{p=1}^{P}(\tau'_{p,1})^2 = r^2\cos^2(\theta)\sum_{p=1}^{P}\frac{\epsilon_p^2}{\beta_p},$$

$$\frac{\lambda^2}{4\pi^2}\sum_{p=1}^{P}(\tau'_{p,2})^2 = P + \sum_{p=1}^{P}\frac{\epsilon_p^2\sin^2(\theta)+1-2\epsilon_p\sin(\theta)}{\beta_p} + 2\sum_{p=1}^{P}\frac{\epsilon_p\sin(\theta)-1}{\sqrt{\beta_p}}$$

$$\frac{\lambda^2}{4\pi^2}\sum_{p=1}^{P}\tau'_{p,1}\tau'_{p,2} = r\cos(\theta)\sum_{p=1}^{P}\epsilon_p\left(\frac{1}{\sqrt{\beta_p}} + \frac{\epsilon_p\sin(\theta)-1}{\beta_p}\right).$$

These sums appear to involve either $1/\beta$ or $1/\sqrt{\beta}$, whose Taylor expansions are obtained subsequently

$$\begin{aligned}\frac{1}{\beta_p} &= 1 + 2\epsilon_p\sin(\theta) + (4\sin^2(\theta)-1)\epsilon_p^2 \\ &\quad - 4\sin(\theta)\cos(2\theta)\epsilon_p^3 \\ &\quad + (1 - 12\sin^2(\theta) + 16\sin^4(\theta))\epsilon_p^4 \\ &\quad + \sin(\theta)[6 - 32\sin^2(\theta) + 32\sin^4(\theta)]\epsilon_p^5 \\ &\quad + [-1 + 24\sin^2(\theta) - 80\sin^4(\theta) + 64\sin^6(\theta)]\epsilon_p^6 \\ &\quad + o\left(\epsilon_p^6\right),\end{aligned}$$

$$\begin{aligned}\frac{1}{\sqrt{\beta_p}} &= 1 + \epsilon_p\sin(\theta) + \frac{3\sin^2(\theta)-1}{2}\epsilon_p^2 \\ &\quad + \sin(\theta)\frac{5\sin^2(\theta)-3}{2}\epsilon_p^3 \\ &\quad + \frac{3 - 30\sin^2(\theta) + 35\sin^4(\theta)}{8}\epsilon_p^4 \\ &\quad + \sin(\theta)\frac{15 - 70\sin^2(\theta) + 63\sin^4(\theta)}{8}\epsilon_p^5 \\ &\quad + \frac{-5 + 105\sin^2(\theta) - 315\sin^4(\theta) + 231\sin^6(\theta)}{16}\epsilon_p^6 \\ &\quad + o\left(\epsilon_p^6\right).\end{aligned}$$

The above expansions are used to obtain Taylor expansion of the different sums appearing in the right hand side of (5). After tedious manipulations, (7), (8), and (9) are obtained in similar fashions. ■

B. Taylor Expansion of the CRB for Arbitrary Arrays: Proof of (10) and (11)

First, note that by replacing r by $\max_p|x_p|/\epsilon$ in the $\mathbf{F}_{ij}$ terms (7)–(9), matrix $\mathbf{F}$ form shown in the equation at the bottom of this page, where for e.g., $b_0^{1,1} = \cos^2(\theta)PS_2/c$. This allows one to obtain, after straightforward algebraic manipulations

$$\begin{aligned}\mathrm{CRB}(\theta) &= [\mathbf{F}^{-1}]_{1,1} \\ &= \frac{1}{b_0^{1,1} - \frac{\left(b_2^{1,1}\right)^2}{b_4^{2,2}}}\left[1 + \epsilon\left(\frac{b_5^{2,2}}{b_4^{2,2}} - \frac{b_0^{1,1}b_5^{2,2} + b_1^{1,1}b_4^{2,2} - 2b_2^{1,2}b_3^{1,2}}{b_0^{1,1}b_4^{2,2} - \left(b_2^{1,1}\right)^2}\right) + o(\epsilon)\right], \\ \mathrm{CRB}(r) &= [\mathbf{F}^{-1}]_{2,2} \\ &= \frac{1}{\epsilon^4 b_4^{2,2}\left(1 - \frac{\left(b_2^{1,1}\right)^2}{b_0^{1,1}b_4^{2,2}}\right)}\left[1 + \epsilon\left(\frac{b_1^{1,1}}{b_0^{1,1}} - \frac{\frac{b_5^{2,2}}{b_4^{2,2}} + \frac{b_1^{1,1}}{b_0^{1,1}} - \frac{2b_2^{1,2}b_3^{1,2}}{b_0^{1,1}b_4^{2,2}}}{1 - \frac{b_2^{1,1}}{b_0^{1,1}b_4^{2,2}}}\right) + o(\epsilon)\right].\end{aligned}$$

By replacing the different terms $b_k^{i,j}$ by their respective values, and after simple but tedious manipulations, we ultimately prove (10) and (11). ■

$$\mathbf{F} = \begin{bmatrix} b_0^{1,1} + b_1^{1,1}\epsilon + b_2^{1,1}\epsilon^2 + o(\epsilon^2) & b_2^{1,2}\epsilon^2 + b_3^{1,2}\epsilon^3 + o(\epsilon^3) \\ b_2^{1,2}\epsilon^2 + b_3^{1,2}\epsilon^3 + o(\epsilon^3) & \epsilon^4\left[b_4^{2,2} + b_5^{2,2}\epsilon + b_6^{2,2}\epsilon^2 + o(\epsilon^2)\right] \end{bmatrix}$$

C. Taylor Expansion of the CRB for Centro-Symmetric Arrays: Proof of (15) and (16)

We use the same approach as in Section B. On one hand, for $S_3 = 0$, we rewrite (12)–(14) as (25) shown at the bottom of this page, leading to

$$\mathrm{CRB}(\theta) = [\mathbf{F}^{-1}]_{1,1} = \frac{1}{b_0^{1,1}}\left[1 - \epsilon^2\left(\frac{b_2^{1,1}}{b_0^{1,1}} - \frac{\left(b_3^{1,2}\right)^2}{b_0^{1,1}b_4^{2,2}}\right) + o(\epsilon^2)\right].$$

If we further impose $S_5 = 0$, (25) further simplifies to

$$\mathbf{F} = \begin{bmatrix} b_0^{1,1} + b_2^{1,1}\epsilon^2 + o(\epsilon^2) & b_3^{1,2}\epsilon^3 + o(\epsilon^3) \\ b_3^{1,2}\epsilon^3 + o(\epsilon^3) & \epsilon^4\left[b_4^{2,2} + b_6^{2,2}\epsilon^2 + o(\epsilon^2)\right] \end{bmatrix}$$

which eventually leads to

$$\mathrm{CRB}(r) = [\mathbf{F}^{-1}]_{2,2} = \frac{1}{\epsilon^4 b_4^{2,2}}\left[1 - \epsilon^2\left(\frac{b_6^{2,2}}{b_4^{2,2}} - \frac{\left(b_3^{1,3}\right)^2}{b_0^{1,1}b_4^{2,2}}\right) + o(\epsilon^2)\right].$$

Replacing the different terms $b_k^{i,j}$ by their values, (15) and (16) are proved after tedious manipulations. ■

D. Proof of the Condition of Centro-Symmetry of Section IV-B

We consider real numbers $x_1, \ldots, x_P$ and form the polynomial $Q(x) \stackrel{\text{def}}{=} (x - x_1)\cdots(x - x_P) \stackrel{\text{def}}{=} x^P - \sigma_1 x^{P-1} + \sigma_2 x^{P-2} + \cdots + (-1)^P \sigma_P$. The coefficients $\sigma_1, \ldots, \sigma_P$, given by $\sigma_k \stackrel{\text{def}}{=} \sum_{1 \le i_1 < i_2 < \cdots < i_k \le P} x_{i_1} x_{i_2} \ldots x_{i_k}$, are known to be linked to $S_1, \ldots, S_P$ defined as $S_k = \sum_{p=1}^{P} x_p^k$ by means of the Newton-Girard formula ([15], pp. 69–74)

$$S_k = \sum_{l=1}^{k-1} (-1)^{l-1} \sigma_l S_{k-l} + (-1)^{k-1} k \sigma_k, k \ge 2 \qquad (26)$$

where by definition $\sigma_{P+1} = \sigma_{P+2} = \cdots = 0$. Let $1, 3, \ldots, 2I + 1$ be all the odd integers $\le P$. Let's assume that $S_1 = S_3 = \cdots = S_{2I+1} = 0$. We will prove that $\sigma_1 = \sigma_3 = \cdots = \sigma_{2I+1} = 0$. We proceed by induction to show that $\sigma_{2i+1} = 0$ for $i = 0, 1, \ldots, I$. This is already verified for $i = 0$ because $\sigma_1 = S_1$. Let's assume $\sigma_1 = \sigma_3 = \cdots = \sigma_{2i+1} = 0$ for some $i \le I$, and let's prove that $\sigma_{2i+3} = 0$. From (26), we have $S_{2i+3} = \sum_{l=1}^{2i+2} (-1)^{l-1} \sigma_l S_{2i+3-l} + (-1)^{2i+2}(2i+3)\sigma_{2i+3}$ is necessarily zero. In fact, $2i+3$ is odd, so that if l is odd, then $2i + 3 - l$ is even and vice versa, for $l = 1, \ldots, 2i + 2$. Also, l and $2i + 3 - l$ both are $\le 2i + 1$ and whenever one is odd, the corresponding σ and S coefficients are zero. Hence, for $l = 1, \ldots, 2i+2$, we have necessarily $\sigma_l S_{2i+3-l} = 0$; and so is σ_{2i+3}. Finally, $Q(x)$ is either $x^P + \sigma_2 x^{P-2} + \sigma_4 x^{P-4} + \cdots + \sigma_P$ if P is even or $x^P + \sigma_2 x^{P-2} + \sigma_4 x^{P-4} + \cdots + \sigma_{P-1} x$ if P is odd. In the first (resp. second) case, zeros of $Q(x)$, i.e., $x_1, \ldots, x_P$, are of the form $\pm\alpha_1, \pm\alpha_2, \ldots$ (resp. $0, \pm\alpha_1, \pm\alpha_2, \ldots$). ■

E. Proof of Inequalities (20)

For arbitrarily chosen $a_1 \le a_2 \le \cdots \le a_P$ and $b_1 \le b_2 \le \cdots \le b_P$, we have $\sum_{i=1}^{P}\sum_{j=1}^{P}(a_i - a_j)(b_i - b_j) \ge 0$ which implies that $P\sum_{i=1}^{P} a_i b_i \ge (\sum_{i=1}^{P} a_i)(\sum_{i=1}^{P} b_i)$, the so-called Tchebychev's sum inequality. If we let $a_i \stackrel{\text{def}}{=} b_i \stackrel{\text{def}}{=} x_i^2$, we obtain $PS_4 \ge S_2^2$ i.e., $\kappa \le 1$. If we let $a_i \stackrel{\text{def}}{=} x_i^2$ and $b_i \stackrel{\text{def}}{=} x_i^4$, we obtain $PS_6 \ge S_2 S_4$ i.e., $\eta \le \kappa$. ■

F. Proof of (21) and (22)

By virtue of (26), we have $S_2 = \sigma_1 S_1 - 2\sigma_2$, $S_4 = \sigma_1 S_3 - \sigma_2 S_2 + \sigma_3 S_1 - 4\sigma_4$ and $S_6 = \sigma_1 S_5 - \sigma_2 S_4 + \sigma_3 S_3 - \sigma_4 S_2 + \sigma_5 S_1 - 6\sigma_6$. If $S_1 = S_3 = S_5 = 0$ (if $P = 4$, only if $S_1 = S_3 = 0$, because this is sufficient to have a centro-symmetric array and automatically implies $S_5 = 0$), and after proper replacement, we obtain $S_6 = 3S_2S_4/4 - S_2^3/8 - 6\sigma_6$ which can be transformed into $3/\kappa = (4/P)(1/\eta) + P/2 + 24P\sigma_6/S_2^3$. By definition, $\sigma_6 = 0$ for $P < 6$ so that the following becomes obvious

$$P = 4, S_1 = S_3 = 0 \rightarrow \frac{3}{\kappa} = \frac{1}{\eta} + 2$$
$$P = 5, S_1 = S_3 = S_5 = 0 \rightarrow \frac{3}{\kappa} = \frac{4}{5}\frac{1}{\eta} + \frac{5}{2}.$$

■

G. κ and η for Large-Sized ULAs

Consider a ULA centered at the origin and made of P sensors spaced by d. The proof is given for odd $P = 2Q + 1$ (extension to even P can be conducted in a similar way). Using the identities of $\sum_{k=1}^{Q} k^\alpha$ for $\alpha = 2, 4$ and 6, we obtain

$$S_2 = 2d^2\sum_{k=1}^{Q} k^2 = d^2\frac{Q(Q+1)(2Q+1)}{3}$$
$$S_4 = 2d^4\sum_{k=1}^{Q} k^4 = d^2\frac{3Q^2+3Q-1}{5}S_2$$
$$S_6 = 2d^6\sum_{k=1}^{Q} k^6 = d^4\frac{3Q^4+6Q^3-3Q+1}{7}S_2$$

which directly implies

$$\kappa = \frac{S_2^2}{PS_4} = \frac{5}{3}\frac{Q(Q+1)}{3Q^2+3Q-1}$$
$$\eta = \frac{S_2^3}{P^2S_6} = \frac{7}{9}\frac{Q^2(Q+1)^2}{3Q^4+6Q^3-3Q+1}.$$

■

$$\mathbf{F} = \begin{bmatrix} b_0^{1,1} + b_2^{1,1}\epsilon^2 + o(\epsilon^2) & b_3^{1,2}\epsilon^3 + o(\epsilon^3) \\ b_3^{1,2}\epsilon^3 + o(\epsilon^3) & \epsilon^4\left[b_4^{2,2} + b_5^{2,2}\epsilon + b_6^{2,2}\epsilon^2 + o(\epsilon^2)\right] \end{bmatrix} \qquad (25)$$

REFERENCES

[1] H. Krim and M. Viberg, "Two decades of array signal processing research," *IEEE Signal Process. Mag.*, vol. 13, no. 4, pp. 67–94, Jul. 1996.

[2] H. Gazzah and S. Marcos, "Cramer-Rao bounds for antenna array design," *IEEE Trans. Signal Process.*, vol. 54, no. 1, pp. 336–345, Jan. 2006.

[3] E. Grosicki, K. Abed-Meraim, and Y. Hua, "A weighted linear prediction method for near field source localization," *IEEE Trans. Signal Process.*, vol. 53, no. 10, pp. 3651–3660, Oct. 2005.

[4] M. N. El Korso, R. Boyer, A. Renaux, and S. Marcos, "Conditional and unconditional Cramer Rao bounds for near-field source localization," *IEEE Trans. Signal Process.*, vol. 58, no. 5, pp. 2901–2906, May 2010.

[5] Y. Begriche, M. Thameri, and K. Abed-Meraim, "Exact Cramer Rao bound for near field source localization," in *Proc. Int. Conf. Inf. Sci., Signal Process. Appl.*, 2012, pp. 718–721.

[6] D. T. Vu, A. Renaux, R. Boyer, and S. Marcos, "A Cramer Rao bounds based analysis of 3D antenna array geometries made from ULA branches," in *Multidimensional Systems and Signal Processing*. Berlin, Germany: Springer-Verlag, Oct. 2011.

[7] M. Gavish and A. J. Weiss, "Array geometry for ambiguity resolution in direction finding," *IEEE Trans. Antennas Propag.*, vol. 39, no. 2, pp. 143–146, Feb. 1991.

[8] A. J. Weiss, A. S. Willsky, and B. C. Levy, "Non uniform array processing via the polynomial approach," *IEEE Trans. Aerosp. Electron. Syst.*, vol. 25, no. 1, pp. 48–55, Jan. 1989.

[9] C. ElKassis, J. Picheral, and C. Mokbel, "Advantages of nonuniform arrays using root-MUSIC," *Signal Process.*, vol. 90, no. 210, pp. 689–695, Elsevier.

[10] Y. Begriche, M. Thameri, and K. Abed-Meraim, "Exact conditional and unconditional Cramer Rao bound for near field localization," in arXiv.

[11] H. Gazzah and J.-P. Delmas, "Spectral efficiency of beamforming-based parameter estimation in the single source case," in *Proc. IEEE SSP*, Nice, 2011, pp. 153–156.

[12] P. Stoica and A. Nehorai, "Performances study of conditional and unconditional direction of arrival estimation," *IEEE Trans. Acoustics, Speech, Signal Process.*, vol. 38, no. 10, pp. 1783–1795, Oct. 1990.

[13] H. Abeida and J.-P. Delmas, "Efficiency of subspace-based DOA estimators," *Signal Process.*, vol. 87, no. 9, pp. 2075–2084, Sep. 2007.

[14] Y. Meurisse and J. P. Delmas, "Bounds for sparse planar and volume arrays," *IEEE Trans. Inf. Theory*, vol. 47, no. 1, pp. 464–468, Jan. 2001.

[15] L. E. Dickson, *Elementary Theory of Equations*. New York, NY, USA: Wiley and Sons, 1914.

Houcem Gazzah was born in Sousse, Tunisia, in 1971. He received the Engineering degree from the *École Supérieure des Communications*, Tunis, Tunisia, in 1995, and the M.Sc. and Ph.D. degrees from the *École Nationale Supérieure des Télécommunications*, Paris, France, in 1997 and 2000, respectively.

He had been a Research Associate with the *Centre National de la Recherche Scientifique* (LSS/Supélec), Gif-sur-Yvette, France (2001–2003); then with the Institute for Digital Communications, at the University of Edinburgh, Edinburgh, U.K. (2004–2006). He is currently an Assistant Professor with the Department of Electrical and Computer Engineering at the University of Sharjah, UAE. His research interests include antenna array signal processing, (blind) channel identification and equalization, multicarriers and OFDM systems, adaptive transmission, and (bit interleaved) coded modulation.

Jean Pierre Delmas (M'00–SM'06) was born in France, in 1950. He received the Engineering degree from Ecole Centrale de Lyon, Écully, France, in 1973, the Certificat d'Etudes Supérieures from Ecole Nationale Supérieure des Télécommunications (ENST), Paris, France, in 1982, and the Habilitation à diriger des recherches (HDR) degree from the University of Paris XI, Orsay, France in 2001.

Since 1980, he has been with Telecom SudParis (formerly INT), where he is presently a Professor in the CITI Department and Director of the UMR CNRS 5157 (SAMOVAR) Laboratory. His teaching and research interests are in the areas of statistical signal processing with application to communications and antenna arrays. He is author and coauthor of more than 100 journal and conference papers and book chapters.

Dr. Delmas has served as an Associate Editor for the IEEE TRANSACTIONS ON SIGNAL PROCESSING from 2002 to 2006 and presently for *Signal Processing* (Elsevier) and the IEEE TRANSACTIONS ON SIGNAL PROCESSING. He is a Member of the Sensor Array and Multichannel Technical Committee of the IEEE Signal Processing Society.